JOURNAL OF MATERIALS SCIENCE 30 (1995) 4817–4822

Electrochemical and microstructural studies of sintered and sintered–plasma nitrided steel containing different alloying elements

N. C. PEREIRA, F. G. MITTELSTÄDT, A. SPINELLI, A. M. MALISKA, A. N. KLEIN, J. L. R. MUZART and C. V. FRANCO*
Departamento de Química, and Departamento de Engenharia Mecânica, Laboratório de Materiais, UFSC, CEP 88040-900, Florianópolis, SC, Brasil

The corrosion of sintered and sintered–plasma nitrided steels containing different alloying elements was evaluated through analysis of the potentiodynamic polarization curves of the samples at pH = 7, with 1.25 M KNO_3 as electrolyte. The Fe–3.0% Ni and Fe–0.1% C sintered alloys show better performance in relation to electrochemical corrosion, than sintered pure iron samples. In addition, Fe–4.0% Mn, Fe–1.5% Mo and Fe–1.5% Si alloys exhibited increased anodic current densities in relation to the pure iron sample. After the nitriding process the anodic current densities of all samples containing an alloying element were considerably diminished. The sintered-nitrided pure iron sample was the only nitrided part whose current density was higher than the current density of the non-nitrided sample.

1. Introduction

Sintered steels have been used in practically all fields of industry owing to their low manufacturing cost. Whilst the mechanical behaviour of these steels has been widely studied, their behaviour regarding corrosion has not yet been studied systematically. Therefore, it was the main aim of this work to contribute to the study of the behaviour of sintered and sintered–plasma nitrided steels, when subjected to electrochemical corrosion. It is well known from conventional metallurgy that thermochemical treatments, besides improving surface hardness and wear and fatigue strength, also improve corrosion strength [1]. In addition, from the literature [2] it is known that in sintered steels the presence of residual pores resulting from the manufacturing process affect their behaviour regarding mechanical loading. Among the available surface treatments of sintered steels, the plasma processes are very promising [3]. Liquid (in molten salts) and gaseous processes are not recommended, because they interact excessively with the internal part through communicating pores. Ionic processes via a plasma do not present this particular problem, but the continuity of the surface layer is compromised in the plasma thermochemical treatment, as in the others. A detailed study of the corrosion strength of sintered and sintered–plasma nitrided steels is necessary in order to elucidate the influence of porosity. As a part of a large project, we present results from a study on sintered alloys with different alloy compositions at constant porosity.

2. Experimental procedure

The binary sintered alloys with the desired chemical composition were obtained using, as a base material, iron powder ASC 100.29. The alloying elements silicon manganese, due to their high affinity for oxygen, were introduced in the form of binary ferroalloys: ferrosilicon with 14.5% Si and ferromanganese with 77.0% Mn. Nickel was added in elementary form, nickel–carbonyl, and molybdenum in the form of ferromolybdenum with 72.5% Mo.

The preparation of the samples was done according to the conventional powder metallurgy pathway, consisting of mixture, compacting and sintering steps under a protective atmosphere. The sample preparation parameters and the resulting composition of each alloy have been established according to the sinterability criteria; these are given in Table I.

Nitriding was processed in a home-made reactor, the sample being connected to the cathode of an abnormal regime discharge. The voltage applied to the cathode was of the order of 450 V, and produces ions and excited species which bombard the sample, causing heating and the nitriding process. Details of the reactor and a description of the peripheral equipment for the control of the nitriding parameters may be found in the literature [3]. The nitriding conditions were as follows: temperature 540 °C, pressure 3 torr (1 torr = 133.322 Pa) time 2 h, voltage 450–470 V, gas mixture composition 75% N_2/25%H_2.

All the reactants utilized in this study were of PA analytical grade, which were dissolved in ultra-pure water obtained by treatment in a Millipore Mille-Q

0022–2461

TABLE I Parameters for the preparation of sintered samples subjected to compacting at 600 MPa

Alloy	Temperature (°C)	Time (h)	Atmosphere
Pure Fe	1150	1.0	H_2 pre-purified
Fe–4.0% Mn	1200	2.0	H_2 ultra pure
Fe–1.5% Si	1200	2.0	H_2 ultra pure
Fe–1.5% Mo	1250	2.0	H_2 ultra pure
Fe–3.0% Ni	1250	2.0	H_2 ultra pure
Fe–0.1% C	1150	1.0	H_2 pre-purified

system. The solution pH was adjusted to 7.0 in a Cole–Parmer, model ChemCadet, pH meter. The electrochemical measurements were performed in a EG & G PARC, model 273A, Galvanostat–potentiostat. Data collection was controlled by a EG & G PARC, model 342C (SoftCorr), via a National Instrument GPIB (General Purpose Interface Board) interface. The corrosion tests were carried out in an electrochemical cell of three electrodes, with the sample under study as the working electrode. Two graphite rods were used as an auxiliary electrode, and one Ag/AgCl (3.0 M NaCl) electrode was used as a reference electrode; however, all the potentials mentioned in the text refer to the normal hydrogen electrode (NHE).

Microstructural analyses of the sintered, nitrided and corroded samples were performed by optical and scanning electron microscopy. Microhardness measurements were performed using scale HV 0.020. X-ray analysis was used for the determination of phases present at the sample surface.

3. Results and discussion

3.1. Microstructure

3.1.1. Microstructure of the sintered material

Owing to the presence of alloying elements and to incomplete homogenization during the sintering process, the microstructure of the sintered samples exhibits several phases, with the exception of the pure iron sample, which presents a totally ferrite structure. When carbon is added to iron, pearlitic regions are established, with an elevated carbon content. Because silicon is a strong ferrite stabilizer, the Fe–1.5% Si alloy is formed of a nearly totally ferrite matrix. The occurrence of a few pearlite islands is due to the presence of carbon (0.4%) in the employed alloy carrier. In the Fe–3.0% Ni alloy, the matrix is predominantly ferrite with small nickel-martensite regions and a few regions of austenite. In the Fe–4.0% Mn alloys, manganese, being an austenite stabilizer and having a small diffusion coefficient, leads to the permeation of manganese martensite in elevated concentrations. Owing to the small diffusion coefficient, the homogenization of the alloying element is not complete, a predominantly martensitic matrix being formed, with ferrite regions inside the iron particles, where the content of alloying element is small. The Fe–1.5% Mo alloy presents ferrite structure.

3.1.2. Microstructure of alloys after plasma nitriding

The chemical composition and the homogeneity of the matrix determine the behaviour of the nitrided layer. The nitrided layer, in all the treated samples, exhibits a fine superficial layer, which is known as the compound layer, 8–17 μm thick. This layer, as obtained from the diffractograms of the nitrided samples, is formed by γ'-Fe_4N and ε-$Fe_{(2-3)}N$ nitrides. Just beneath the compound layer the diffusion zone is found, where nitrogen is present in interstitial form, such as iron nitrides or of iron nitride needles (Fig. 1).

In the pure iron (Fig. 1a) and Fe–0.1% C samples, the composed layer is very brittle. In the diffusion zone, in spite of the presence of a large number of nitride needles, microhardness measurements have shown a small increase in hardness. A similar behaviour was observed for the Fe–3.0% Ni (Fig. 1b) alloy. In this case, however, no brittleness of the compound layer was observed.

For the Fe–1.5% Si (Fig. 1c) alloy, as presented by Maliska *et al.* [4], the compound layer penetrates through the particle boundaries next to the surface. This fact is probably due to the presence of silicon-rich liquid phase during the sintering process, which leads to an increase of the silicon content at the particle boundaries. This contour-penetrating compound layer also involves the pearlite grains situated in the region next to the surface. Pearlite, situated further away from the diffusion zone, has a tendency to precipitate nitride needles, probably Fe_4N. Additionally electron scanning microscopy has revealed that other nitrides are finely dispersed next to these needles.

Although the Fe–1.5% Si alloy presented higher values of compound layer microhardness, with the compound layer penetrating more deeply through the boundaries next to the surface, microhardness measurements show that grains in the diffusion zone are not hardened, as is evident from microhardness impressions. Even grains with nitride needle precipitates have been hardened very little, probably due to the large distance between the nitride needles. The diffusion zone in this alloy is thus limited not by the microhardness values, but by the presence of the nitride needle. These needles exist up to a depth of 500 μm.

The Fe–1.5% Mo sample after nitriding presents a microstructure similar to the Fe–1.5% Si sample, although the layer growth along the grain and particle boundaries is not as pronounced; In addition, the depth of the white layer is smaller.

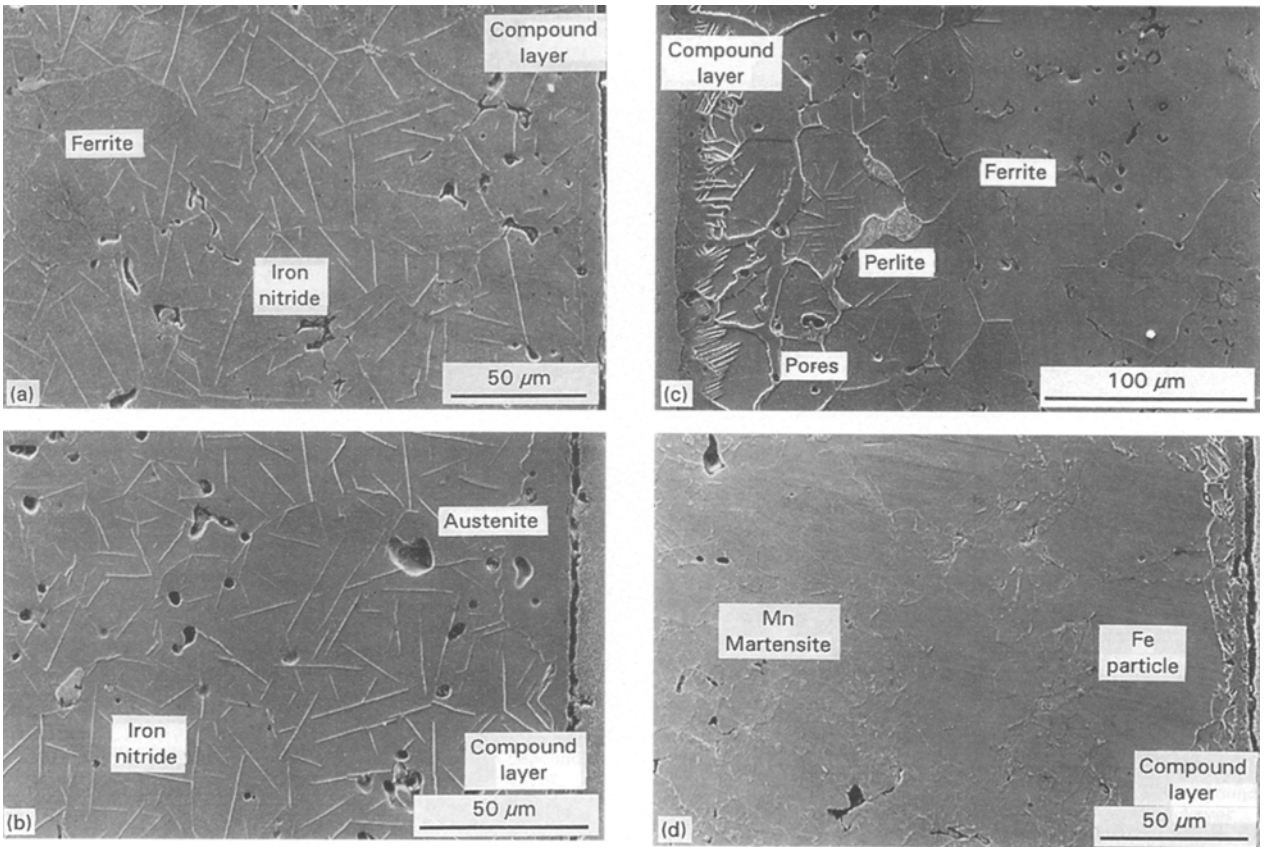

Figure 1 Microstructure of alloys after 2.0 h plasma nitriding. (a) Pure Fe, (b) Fe–3.0% Ni; (c) Fe–1.5% Si; (d) Fe–4.0% Mn.

From optical micrographs of the ion-nitrided layer of Fe–4.0% Mn alloy (Fig. 1), the presence of the superficial compound layer is clearly observed. However, microhardness measurements reveal the existence of an intermediate hardened region between the compound layer and the nucleus of the sample. Probably, this diffusion zone is hardened by the presence of finely dispersed manganese nitrides. Owing to its high alloy proportion and nitride features, manganese may give rise to the formation of manganese nitrides during the nitriding processes. Some ferrite grains situated next to the compound layer have precipitates of iron nitride needles, owing to the small amount of the alloying element in the ferrite.

In alloys containing manganese, the diffusion zone was defined by the microhardness values, because only some of the larger ferrite grains next to the periphery exhibit needle-like precipitates, and were only slightly hardened. The microhardness profiles of this nitrided alloy exhibit homogeneous hardening and a gradual loss of hardness as a function of distance from the surface.

The morphology of the sintered and nitrided sample surface was examined by scanning electron microscopy (Fig. 2). The basic change observed in the topography of the treated samples is the appearance of a granular outgrowth. This makes the visualization of the grain boundaries difficult. In addition, depending on the alloy composition, there is a variation in this granularity. This can be related to the larger number of γ' and ε phases which are present in the compound layer, as determined by the X-ray analysis.

3.2. Electrochemistry

3.2.1. E_{corr} versus time tests

All the samples used in this work were initially submitted to E_{corr} versus time tests for a 30 min period, a length of time which has been defined in order to reach the electric equilibrium of metal and solution. Fig. 3 a and b show the profiles of the E_{corr} versus time curves for several sintered and sintered–nitrided alloys. All tests were performed at pH = 7, using 1.25 M KNO_3 as support electrolyte. From Fig. 3a it is seen that the corrosion potential of the sintered parts after immersion for 30 min is much more active than the potential developed by the same parts immediately after immersion in the aggressive medium. This is a characteristic behaviour of metals under active open circuit corrosion, when not covered by an oxide film and thus suggesting that sintered parts obey the same law. The corrosion potential of sintered–nitrided Fe–3.0% Ni, Fe–0.1% C and pure iron (Fig. 3b) is not significantly displaced, being nearly constant during the 30 min immersion. The corrosion potential of the Fe–1.5% Mo, Fe–4.0% Mn and Fe–1.5% Si is shifted to less nobler potential values. Comparing values of the corrosion potential of sintered and sintered–nitrided metallic alloys (Table II), it is observed that the corrosion potential of sintered–nitrided Fe–3.0% Ni and Fe–0.1% C alloys has been shifted to nobler regions, whilst that of the Fe–1.5% Si alloy and of the pure iron sample (sintered–nitrided) shifted to the cathodic region. No significant changes occurred in the E_{corr} value of the other sintered–nitrided alloys. These tests indicate, at first sight, that the nitriding

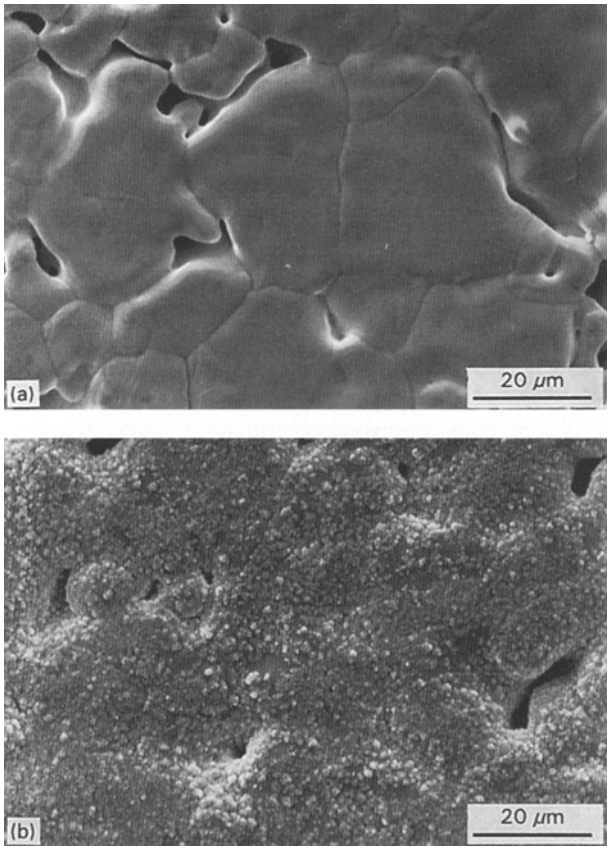

Figure 2 Surface aspect of Fe–3.0% Ni alloy samples, under the electron microscope; (a) sintered, (b) plasma nitrided.

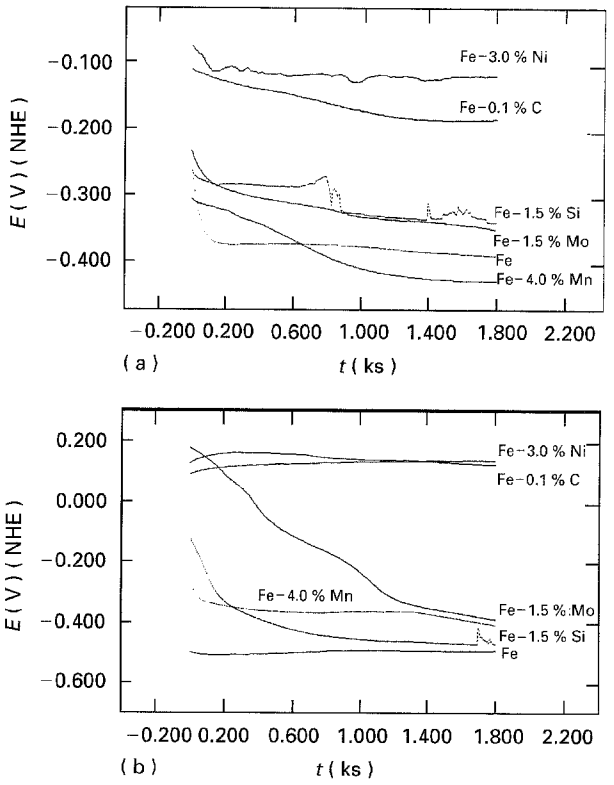

Figure 3 E_{corr} versus time curves of (a) sintered steels, (b) sintered–nitrided steels.

process reduces the open circuit corrosion susceptibility, and mainly for those alloys whose corrosion potential has been shifted towards nobler values.

3.2.2. Potentiodynamic tests

After the E_{corr} versus time tests, the potentiodynamic curves for each metallic alloy were plotted, the anodic sweep being started for potentials slightly lower than the corresponding corrosion potentials, and concluded after crossing the metal's transpassivation region. Fig. 4a–f are E–log$I$ graphs for each case. In order to compare the corrosion activity of the sintered and sintered–nitrided parts, an arbitrary potential was chosen, 0.2 V above the corrosion potential of each alloy and, at this potential, the current density resulting from polarization was measured. This potential is, in all cases, situated inside the active dissolution region of the alloy. The results obtained are shown in Table III.

With the exception of the pure iron sample (Fig. 4c), all the other sintered–nitrided samples show anodic dissolution current densities which are slightly below those of sintered parts. Only the potentiodynamic polarization curves of the sintered samples show a profile similar to an ideal polarization curve (Fig. 5), containing active, passive and transpassive regions. In polarization curves of the sintered–nitrided samples, an increase is observed in the current densities, as a function of the applied potential. However, the profile of these curves does not allow a delimitation into active, passive and transpassive regions. The increase

TABLE II E_{corr} (V) (NHE) values obtained in 1.25 M KNO_3 medium

Alloy	E_{corr} (V)	
	Sintered	Sintered–nitrided
Fe–3.0% Ni	– 0.1250	+ 0.1120
Fe–0.1% C	– 0.1840	+ 0.1350
Pure Fe	– 0.3970	– 0.4960
Fe–4.0% Mn	– 0.4250	– 0.4180
Fe–1.5% Mo	– 0.3550	– 0.3990
Fe–1.5% Si	– 0.3130	– 0.4760

of the current density as a function of the applied potential may be related to a mass transfer process. A comparison of the current densities for sintered and sintered–nitrided alloys (Table III) shows that the nitriding processes reduce the anodic current density [3] by a factor of approximately 60 times (measured 0.2 V above the potential corrosion) for the Fe–1.5% Si alloy, 15 times for the Fe–4.0% Mn alloy, 10 for the Fe–3.0% Ni alloy, 3.5 for the Fe–0.1% C alloy and 2.5% for the 1.5% Mo alloy, when compared with the current densities of the same alloys, when only sintered. The only sintered–nitrided sample whose current density was higher than that of the corresponding sintered sample was pure iron. In a preliminary analysis it may thus be said that nitriding reduces the corrosion activity of the samples containing some alloying element. The effect of each alloying element may be better visualized by comparing the anodic current density of the sintered and sintered–nitrided parts containing some alloying element with the pure iron sample. The sintered Fe–3.0% Ni alloy has a den-

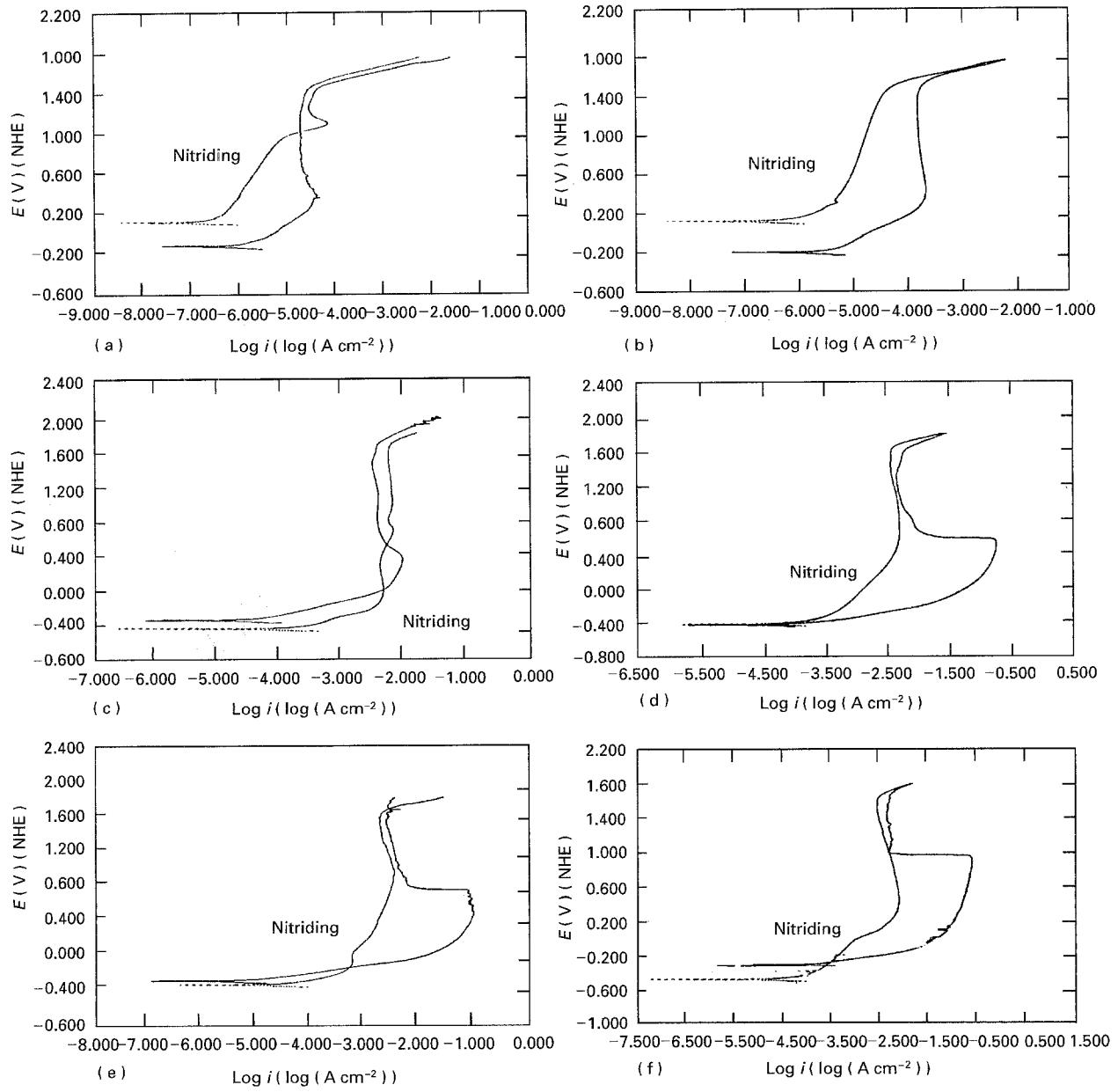

Figure 4 Potentiodynamic polarization curves for the different sintered and sintered–nitrided alloys in 1.25 M KNO_3 medium; 25°C; scan rate of 0.8 mV s^{-1}; (a) Fe–3.0% Ni; (b) Fe–0.1% C; (c) pure Fe; (d) Fe–4.0% Mn; (e) Fe–1.5% Mo; (f) Fe–1.5% Si.

TABLE III i (A cm^{-2}) values measured 0.2 V above E_{corr}

	i (A cm^{-2})	
Alloy	Sintered	Sintered–nitrided
Fe–3.0% Ni	7.8×10^{-6}	7.8×10^{-7}
Fe–0.1% C	1.7×10^{-5}	4.8×10^{-6}
Pure Fe	7.1×10^{-4}	2.3×10^{-3}
Fe–4.0% Mn	9.0×10^{-3}	6.0×10^{-4}
Fe–1.5% Mo	1.5×10^{-3}	5.8×10^{-4}
Fe–1.5% Si	1.9×10^{-2}	3.2×10^{-4}

sity current which is 90 times smaller than the pure iron sample. After nitriding, the alloy had a current density 3000 times smaller than the pure iron sample. The Fe–0.1% C, which exhibited a current density nearly 40 times smaller than that of iron, showed a current density 480 times smaller than that of iron after nitiriding. The Fe–4.0% Mn, Fe–1.5% Mo and Fe–1.5% Si sintered alloys, had current densities 12, 2 and 27 times larger than that of sintered pure iron. After nitriding, the respective alloys current densities were, 4, 4 and 7 times smaller, respectively, than the sintered–nitrided pure iron sample. These results indicate that nitriding may be an efficient protection against corrosion in 1.25 M KNO_3 medium. The influence of each alloying element in the corrosion of nitrided and non-nitrided parts needs further detailed study; however, it is perceivable that the presence of these elements improves efficiency against corrosion of sintered–nitrided parts. The same behaviour is not observed in all sintered alloys.

The potentiodynamic studies on the sintered–nitrided Fe–3.0% Ni alloy (Fig. 4a) show the appearance of an anodic current peak at 1.14 V, with a current density of 7.1×10^{-5} A cm^{-2}. This peak has been observed previously in our laboratory [5], in studies with other metal alloys. Studies using cyclic voltammetry performed with pure nickel in alkaline medium

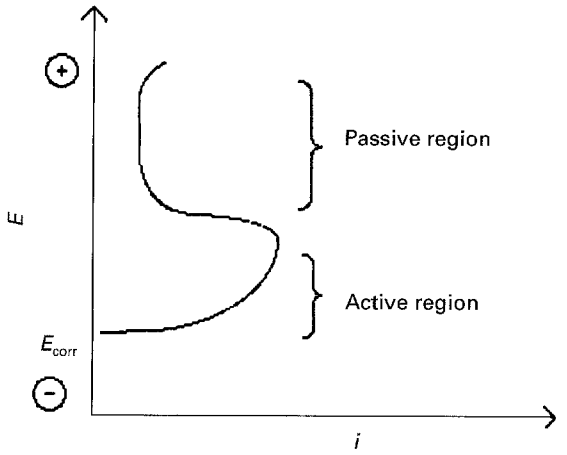

Figure 5 Ideal anodic polarization curve.

[6] have shown that this peak corresponds to the oxidation process $Ni^{2+} \rightarrow Ni^{3+}$. Hahn *et al.* [7, 8], by means of spectroscopy reflectance studies, have shown that only the β-$Ni(OH)_2$ species is a precursor of the formation of superior oxides of the type NiOOH or $Ni_2O_3 \cdot H_2O$. These models may perhaps be applicable to our case. However, additional studies are required in order to explain why this behaviour is only observed with nitrided parts.

Fig. 6 shows the surface aspect of Fe–3.0% Ni alloy samples before and after being exposed to corrosion. It is observed that dissolution occurs preferentially in the pores and along the contacts formed between particles during sintering. As a consequence of corrosion preceding preferentially at regions where the nitrided layer is interrupted, the pore volume increases, thus allowing the access of reactants to the metal base. Thus, nitriding in sintered steels does not produce an effective passivation as occurs with conventional steel [5]. The amount of passivation depends on the degree of discontinuity of the nitrided layer which, in turn, depends on the kinetic growth of the layer, and the size and pore content of the steel.

4. Conclusion

Preliminary electrochemical studies to characterize the corrosion behaviour of sintered–plasma nitrided steels in KNO_3 medium reveal the following observations: the alloying elements nickel and carbon reduce the corrosion process of these sintered steels, whilst the elements manganese molybdenum and silicon act in the other sense. Nitriding considerably reduces the corrosion activity of all tested samples containing some alloying element. These results are evident when the performance of the alloys is compared with that of pure iron. When the influence of the alloying elements on sample corrosion of sintered–nitrided samples is compared, the following decreasing order of protection is found: Fe–3.0% Ni $\gg$ Fe–0.1% C $\gg$ Fe–1.5% Si $>$ Fe–1.5% Mo $\approx$ Fe–4.0% Mn $\gtrsim$ Fe. Surface analysis using scanning electron microscopy has confirmed these results, which were obtained by electrochemistry.

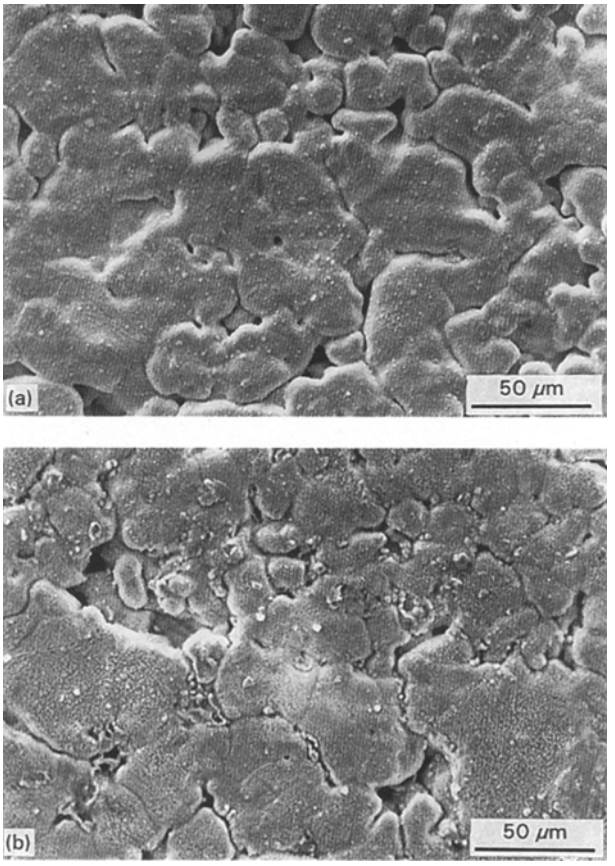

Figure 6 Electron micrographs of the nitrided Fe–4.0% Mn (a) before, and (b) after the corrosion test.

Acknowledgements

The authors wish to thank FINEP, PADCT and FUNCITEC for financial support.

References

1. D. J. ORZESKE, *Ind. Heat.* **53** (1986) 34.
2. K. RAZAVIZADEH and B. L. DAVIES, *Powder Metall* **22** (1979) 187.
3. L. C. FONTANA, V. DRAGO, A. V. BRAND, A. R. SOUZA and J. L. R. MUZART, *Brazilian J. Vac. Applic.* **9** (1990) 69.
4. A. M. MALISKA, A. N. KLEIN and A. R. SOUZA, *Anais do XII Congresso Brasileiro de Engenharia Mecânica* **3** (1993) 1723.
5. F. G. MITTELSTÄDT, Master dissertation, Department of Chemistry, The Federal University of Santa Catarina, Brasil (1993).
6. D. FLONER, Doctoral thesis, University of Poitiers, France (1988).
7. F. HAHN, Thèse de Doctorat de Troisième Cycle, University of Poitiers, France (1984)
8. F. HAHN, B. BEDEN M.-J. CROISSANT and C. LAMY, *Electrochim. Acta* **31** (1986) 335.

Received 22 December 1994
and accepted 28 April 1995